Tunable Novel Cyclopentadithiophene-Based Copolymers Containing Various Numbers of Bithiazole and Thienyl Units for Organic Photovoltaic Cell Applications

ARTICLE *in* MACROMOLECULES · JUNE 2009

Impact Factor: 5.8 · DOI: 10.1021/ma900416d

8 AUTHORS, INCLUDING:

Po-Ju Huang
University of California, Santa Barbara
2 PUBLICATIONS **85** CITATIONS
SEE PROFILE

Chih Wei Chu
Academia Sinica
169 PUBLICATIONS **4,484** CITATIONS
SEE PROFILE

Kung-Hwa Wei
National Chiao Tung University
172 PUBLICATIONS **6,204** CITATIONS
SEE PROFILE

Hong-Cheu Lin
National Chiao Tung University
155 PUBLICATIONS **2,437** CITATIONS
SEE PROFILE

Tunable Novel Cyclopentadithiophene-Based Copolymers Containing Various Numbers of Bithiazole and Thienyl Units for Organic Photovoltaic Cell Applications

Kuang-Chieh Li,[†] Jen-Hsien Huang,[§] Ying-Chan Hsu,[‡] Po-Ju Huang,[†] Chih-Wei Chu,[∥,⊥] Jiann-T'suen Lin,[‡] Kuo-Chuan Ho,[§] Kung-Hwa Wei,[†] and Hong-Cheu Lin*[,†]

Department of Materials Science and Engineering, National Chiao Tung University, Hsinchu, Taiwan (ROC), Institute of Chemistry, Academia Sinica, Taipei, Taiwan (ROC), Department of Chemical Engineering, National Taiwan University, Taipei, Taiwan (ROC), Research Center for Applied Sciences, Academia Sinica, Taipei, Taiwan (ROC), and Department of Photonics, National Chiao Tung University, Hsinchu, Taiwan (ROC)

Received February 24, 2009; Revised Manuscript Received March 31, 2009

ABSTRACT: Six novel conjugated copolymers (**P1**−**P6**) containing coplanar cyclopentadithiophene (CPDT) units (incorporated with bithiazole/thienyl-based monomers) were synthesized and developed for the applications of polymer solar cells (PSCs). Copolymers **P1**−**P6** covered broad absorption ranges from UV to near-infrared (400−800 nm) with narrow optical band gaps of 1.70−1.94 eV, which are compatible with the maximum solar photon reflux. Partially reversible p- and n-doping processes of **P1**−**P6** in electrochemical experiments were observed. Compared with those previously reported CPDT-based narrow band gap polymers, the proper molecular design for HOMO/LUMO levels of **P1**−**P6** induced relatively high photovoltaic open-circuit voltages in the PSC devices. Powder X-ray diffraction (XRD) analyses suggested that these copolymers formed highly self-assembled $\pi-\pi$ stackings. Under 100 mW/cm^2 of AM 1.5 white-light illumination, bulk heterojunction PSC devices containing an active layer of electron donor copolymers **P1**−**P6** blended with electron acceptor [6,6]-phenyl C_{61} butyric acid methyl ester (PCBM) in the weight ratio of 1:1 were explored, and the external quantum efficiency (EQE) measurements showed a maximal quantum efficiency of 60%. The PSC device containing **P4** in the weight ratio of 1:2 with PCBM gave the best preliminary result with an overall power conversion efficiency (PCE) of 3.04%, an open-circuit voltage of 0.70 V, a short-circuit current of 8.00 mA/cm^2, and a fill factor of 53.7%.

Introduction

Extensive researches in the field of electro-optical devices have been focused on soluble π-conjugated semiconducting polymers, especially for the developments of organic photovoltaic (OPV) devices, which offer the advantages of lightweight, high-throughput, and environmentally renewable energy for future applications. Since the pioneering achievements of A. J. Heeger and co-workers in 1995,[1] the so-called bulk heterojunction (BHJ) concept has significantly improved the power conversion efficiency (PCE) values of the OPV devices, where interpenetrating electron donor−acceptor (D-A) networks were formed by blending phase-separated π-conjugated polymers (as electron donors) with soluble fullerenes, strong electron-affinity polymers,[2] or n-type nanocrystals[3] (as electron acceptors). For the electron-donating purpose, an increasing interest for novel polymeric materials with high charge carrier mobility and good processability has recently been found in thiophene-based conducting copolymers, such as derivatives of region-regular poly(3-hexylthiophene)s (P3HTs),[4] polythiophenes,[5] and fused heterocyclic conjugated polymers,[6] etc., resulting in OPV devices with the highest PCE value approaching 5.0%.

Recently, in order to obtain longer conjugation lengths, more planar molecular geometries, and more rigid structures in π-conjugated polymers,[7] novel heteroaromatic fused-ring derivatives, including cyclopentadithiophene (CPDT) units, have been widely investigated in PSCs. Kraak et al. first reported the structural unit of CPDT in 1968,[8a] and the later prepared CPDT-based polymers showed relatively high conductivities[8b,c,9a] due to the more extensive π-conjugation lengths as compared with polythiophene and polyfluorene derivatives.[9] These enhanced photovoltaic properties of CPDT-based polymers have been found to be a powerful approach to optimizing the PSC performance, and thus to lower HOMO−LUMO band gaps and enable closer intermolecular interactions, resulting from the increases of coplanarities and longer conjugation lengths. Lately, the derivatives of cyclopentadithiophene-based copolymers have been emerged as very promising materials for OPV devices which possess both prominent properties of high carrier mobility[6c,10] and improved power conversion efficiency (PCE).[10b,11]

Furthermore, a novel class of π-conjugated polymers composed of five-membered heteroaromatic rings with alkyl side chains, i.e., poly(alkylbithiazole)s, have a strong tendency to self-assemble into stacked solid structures, and they exhibit interesting thermochromic and electrochemical behavior.[12,13,14b] These conjugated polymers containing five-membered rings were considered to possess more coplanar structures and form more highly extended π-conjugated systems owing to their less sterically hindered structures compared with those containing six-membered rings. The thiazole unit is one of the strongest electron-accepting azaheterocycles because it contains one electron-withdrawing nitrogen of imine (−C═N) in place of the carbon atom at the 3-position of thiophene. Therefore, π-conjugated polymers incorporating with bithiazole (BT) moieties have been demonstrated to be as new n-type transporting materials.[12,13] However, only a limited number of bithiazole-based polymers have been explored, and their applications in PSC devices were quite rare.[14]

* Author for correspondence. Telephone: 8863-5712121 ext. 55305. Fax: 8863-5724727. E-mail: linhc@cc.nctu.edu.tw.
[†] Department of Materials Science and Engineering, National Chiao Tung University.
[‡] Institute of Chemistry, Academia Sinica.
[§] Department of Chemical Engineering, National Taiwan University.
[∥] Research Center for Applied Sciences, Academia Sinica.
[⊥] Department of Photonics, National Chiao Tung University.

10.1021/ma900416d CCC: $40.75
Published on Web 04/22/2009

The band-gaps along with the HOMO and LUMO levels of the conjugated polymers are finely tunable by copolymerization of different monomer units.[6a,14b,15] Another important observation was found that the electron-withdrawing cyano groups could decrease the HOMO level and thus to stabilize the neutral state of the conjugated system.[15] These results suggest that it is necessary to investigate the effects of copolymerized functional units on the optical, electrochemical, and PSC properties of the π-conjugated polymers.

On the basis of this electron donor−acceptor (D−A) concept, six different bithiazole-based monomers, i.e., oligo(bithiazole)s **M1**−**M3**, bithiazole−oligo(thiophene)s **M4**−**M5**, and diarylene−cyanovinylene−bithiazole **M6**, were utilized as electron acceptor moieties to synthesize CPDT−BT-based copolymers **P1**−**P6**. Therefore, our donor−acceptor approaches utilized in the solid films of the CPDT−BT-based copolymers (**P1**−**P6**) achieve the absorption spectra in the visible range of 300−800 nm (with tailing up to around 900 nm) possessing narrow electrochemical band gaps of 1.51−1.83 eV. In addition, the molecular configurations of the π-conjugated CPDT−BT-based copolymers could clearly ensured that highly organized $\pi-\pi$ stackings could be easily generated in these fused-heteroaromatic molecular frameworks by thermal annealing, which were confirmed by the powder X-ray diffraction (XRD) analyses. They also showed good charge-transporting properties with hole mobilities of $(3.3-5.6) \times 10^{-4}$ cm^2V^{-1} s^{-1} and fair processabilities for PSC applications. So far, the preliminary PSC performance of these structurally related copolymers showed the best PCE value up to 3.04% while blended with [6,6]-phenyl C_{61} butyric acid methyl ester (PCBM), with a short circuit current density (I_{sc}) of 8.00 mA/cm^2, an open circuit voltage (V_{oc}) of 0.70 V, and a fill factor (FF) of 53.7% under AM 1.5 (100 mW/cm^2).

Experimental Section

Materials. All chemicals and solvents were reagent grades and purchased from Aldrich, ACROS, Fluka, TCI, and Lancaster Chemical Co. Toluene, tetrahydrofuran, and diethyl ether were distilled to keep anhydrous before use. If not otherwise specified, the other solvents were degassed by nitrogen 1 h prior to use. All of the other chemicals were used as received.

Measurements and Characterization. ^{1}H NMR spectra were recorded on a Varian Unity 300 MHz spectrometer using $CDCl_3$ solvents. Elemental analyses were performed on a HERAEUS CHN-OS RAPID elemental analyzer. Transition temperatures were determined by differential scanning calorimetry (DSC, Perkin-Elmer Pyris 7) with a heating and cooling rate of 10 °C/min. Thermogravimetric analyses (TGA) were conducted with a TA Instruments Q500 at a heating rate of 20 °C/min under nitrogen. Gel permeation chromatography (GPC) analyses were conducted on a Waters 1515 separation module using polystyrene as a standard and THF as an eluant. UV−visible absorption and photoluminescence (PL) spectra were recorded in dilute chloroform solutions (10^{-6} M) on a HP G1103A and Hitachi F-4500 spectrophotometer, respectively. Solid films of UV−vis and PL measurements were spin-coated on a quartz substrate from chlorobenzene solutions with a concentration of 10 mg/mL. Cyclic voltammetry (CV) measurements were performed using a BAS 100 electrochemical analyzer with a standard three-electrode electrochemical cell in a 0.1 M tetrabutylammonium hexafluorophosphate ((TBA)PF_6) solution (in acetonitrile) at room temperature with a scanning rate of 50 mV/s. During the CV measurements, the solutions were purged with nitrogen for 30s. In each case, a carbon working electrode coated with a thin layer of copolymers, a platinum wire as the counter electrode, and a silver wire as the quasi-reference electrode were used, and Ag/AgCl (3 M KCl) electrode was served as a reference electrode for all potentials quoted herein. The redox couple of ferrocene/ferrocenium ion (Fc/Fc^+) was used as an external standard. The corresponding highest occupied molecular orbital (HOMO) and lowest unoccupied molecular orbital (LUMO) levels were calculated using $E_{ox/onset}$ and $E_{red/onset}$ for experiments in solid films of copolymers **P1**−**P6**, which were performed by drop-casting films with the similar thickness from THF solutions (ca. 5 mg/mL). The LUMO level of PCBM employed was in accordance with the literature datum.[16b] The onset potentials were determined from the intersections of two tangents drawn at the rising currents and background currents of the cyclic voltammetry (CV) measurements. Synchrotron powder X-ray diffraction (XRD) measurements were performed at the beamline BL17A of the National Synchrotron Radiation Research Center (NSRRC), Taiwan (for details of the XRD installation, see Supporting Information).

Device Fabrication and Characterization of Polymer Solar Cells (PSCs). The polymer photovoltaic (PV) cells in this study were composed of an active layer of blended copolymers (**P1**−**P6**:PCBM) in solid films, which was sandwiched between a transparent indium tin oxide (ITO) anode and a metal cathode. Prior to the device fabrication, ITO-coated glass substrates (1.5×1.5 cm^2) were ultrasonically cleaned in detergent, deionized water, acetone, and isopropyl alcohol. Afterward, the substrates were treated with UV ozone for 15 min, and a layer of poly(ethylene dioxythiophene):polystyrenesulfonate (PEDOT:PSS, ~30 nm) was subsequently spin-coated onto the substrates. After baking at 130 °C for one hour, the substrates were transferred to a nitrogen-filled glovebox. The PSC devices were fabricated by spin-coating solutions of blended copolymers **P1**−**P6**:PCBM (with various weight ratios) onto the PEDOT:PSS modified substrates at 600 rpm for 60 s (ca. 200 nm), and placed in a covered glass Petri dish. Initially, the blended solutions were prepared by dissolving both copolymers (**P1**−**P6**) and PCBM (with a 1:1 weight ratio initially and then with various weight ratios for the optimum copolymer) in DCB (20 mg/1 mL), followed by continuous stirring for 12 h at 50 °C. In the slow-growth approach, blended copolymers in solid films were kept in the liquid phase after spin-coating by using the solvent with a high boiling point. Finally, a calcium layer (30 nm) and a subsequent aluminum layer (100 nm) were thermally evaporated through a shadow mask at a pressure below 6×10^{-6} Torr, and the active area of the device was 0.12 cm^2. All PSC devices were prepared and measured under ambient conditions. In the hole-only devices,[17a] the calcium layer was replaced with a MoO_3 ($\Phi = 5.3$ eV) layer, which has been shown to provide a good hole injection contact in PSC devices containing copolymers **P1**−**P6**. The MoO_3 layer with a thickness of 20 nm was thermally evaporated and then capped with 50 nm of Al.

Synthesis. Excepting compounds 4,4′-dihexyl-2,2′-bithiazole (**1**),[14a] thiophen-2-yl-2-boronic acid (**7**),[18] and 4*H*-cyclopenta [2,1-*b*:3,4-*b*′]dithiophene (**12**),[19] which were synthesized according to the known literature procedures, the detailed synthetic procedures of the other precursors are shown in the Supporting Information. The monomers **M1**−**M6** and copolymers **P1**−**P6** are shown in Schemes 1, 2, and 3, respectively, and their synthetic procedures are described as follows.

*5,5′-Dibromo-4,4′-dihexyl-2,2′-bithiazole (***M1***).* Compound **1** (4.7 g, 14.2 mmol) was dissolved in a mixture of *N,N*-dimethylformamide (30 mL) and glacial acetic acid (30 mL) under nitrogen in the dark, and then NBS (6.3 g, 35.6 mmol) was added dropwise. After 2 h of stirring in the dark, a white crude solid was precipitated in the reaction mixture. The precipitate was filtered, washed with methanol, and then purified by column chromatography with CH_2Cl_2/hexane (1:3) to obtain the dibromo product (6.5 g). Yield: 92%. ^{1}H NMR (ppm, $CDCl_3$): δ 2.72 (t, $J = 7.2$ Hz, 4H), 1.68 (m, 4H), 1.31 (m, 12H), 0.87 (t, $J = 7.2$ Hz, 6H). ^{13}C NMR (ppm, $CDCl_3$): δ 159.90 (2C), 157.35 (2C), 106.80 (2C), 31.54 (2C), 29.47 (2C), 28.80 (2C), 28.62 (2C), 22.57 (2C), 14.06 (2C). MS (FAB): *m*/*z* [M^+] 495; calcd *m*/*z* [M^+] 494.0. Anal. Calcd for $C_{18}H_{26}Br_2N_2S_2$: C, 43.73; H, 5.30; N, 5.67; S, 12.97. Found: C, 43.66; H, 5.36; N, 5.75; S, 13.14.

M2. Compound **5** (1.7 g, 2.6 mmol) was dissolved in a mixture of *N,N*-dimethylformamide (30 mL) and chloroform (30 mL) in the dark. NBS (1.2 g, 6.3 mmol) was added dropwise and the reacted solution was heated at 70 °C for 3 h under nitrogen. After

Scheme 1. Synthetic Routes of Oligo(bithiazole)-Based Monomers M1−M3

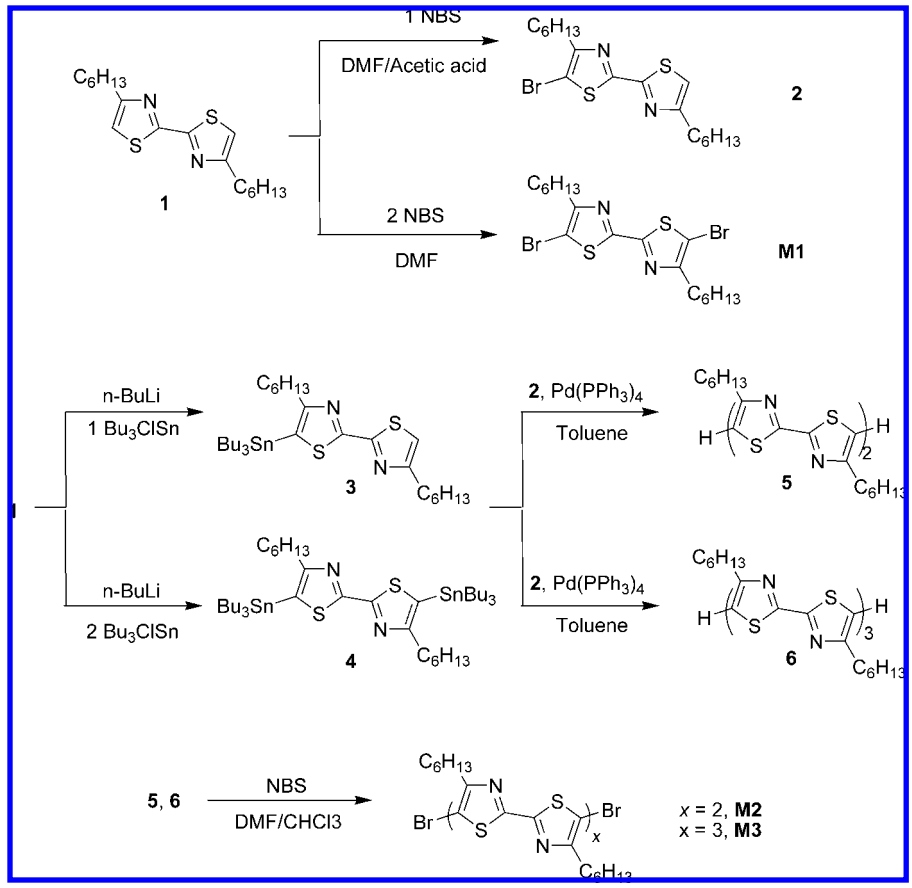

cooling to room temperature, the reaction was stopped under reduced pressure and a red crude solid was precipitated in the mixture. The precipitate was filtered, washed with methanol, and then purified by column chromatography with CH_2Cl_2/hexane (2:5) to attain the dibromo product (1.7 g).Yield: 82%. ^{1}H NMR (ppm, $CDCl_3$): δ 2.77 (t, J = 7.2 Hz, 4H), 2.69 (t, J = 7.2 Hz, 4H), 1.69 (m, 8H), 1.29 (m, 24H), 0.87 (m, 12H).^{13}C NMR (ppm, $CDCl_3$): δ 160.43 (2C), 160.14 (2C), 158.36 (2C), 157.55 (2C), 121.84 (2C), 107.05 (2C), 31.55 (4C), 29.79 (2C), 29.55 (2C), 29.37 (2C), 28.99 (2C), 28.82 (2C), 28.71 (2C), 22.57 (2C), 22.53 (2C), 14.06 (2C), 14.03 (2C). MS (FAB): *m/z* [M^+] 828.0; calcd *m/z* [M^+] 828.1. Anal. Calcd for $C_{36}H_{52}Br_2N_4S_4$: C, 52.16; H, 6.32; N, 6.76; S, 15.47. Found: C, 51.85; H, 6.15; N, 6.61; S, 14.97.

M3. The synthesis of monomer **M3** was followed by a procedure similar to that described for monomer **M2**. Compound **6** (3.0 g, 3.0 mmol) was dissolved in a mixture of *N,N*-dimethylformamide (80 mL) and chloroform (80 mL) in the dark. NBS (1.6 g, 9.0 mmol) was added dropwise, and the reacting solution was heated at 70 °C for 3 h under nitrogen. The crude product was purified by column chromatography with CH_2Cl_2/hexane (2:3) to obtain a red solid (3.1 g). Yield: 90%. ^{1}H NMR (ppm, $CDCl_3$): δ 2.74 (t, J = 7.2 Hz, 4H), 2.71 (t, J = 7.2 Hz, 8H), 1.71 (m, 12H), 1.30 (m, 36H), 0.86 (m, 18H).^{13}C NMR (ppm, $CDCl_3$): δ 160.67 (2C), 160.45 (2C), 160.15 (2C), 158.55 (2C), 158.39 (2C), 157.56 (2C), 122.13 (2C), 121.89 (2C), 107.04 (2C), 31.56 (6C), 29.82 (3C), 29.56 (3C), 29.45 (3C), 29.39 (3C), 29.01 (3C), 28.82 (3C), 28.72 (3C), 22.55 (3C), 14.07 (3C), 14.03 (3C). MS (FAB): *m/z* [M^+] 1163.0; calcd *m/z* [M^+] 1162.3. Anal. Calcd for $C_{54}H_{78}Br_2N_6S_6$: C, 55.75; H, 6.76; N, 7.22; S, 16.54. Found: C, 55.94; H, 6.66; N, 6.99; S, 17.04.

5,5′-Di(5-bromothiophene-2-yl)-4,4′-dihexyl-2,2′-bithiazole (**M4**). Compound **8** (3.0 g, 6.0 mmol) was dissolved in chloroform (100 mL) under nitrogen, and then *N*-bromosuccinimide (2.2 g, 12.1 mmol) was added finally. After refluxing the reaction mixture for 4 h, the product was poured into water (200 mL). The solution was extracted with dichloromethane (100 mL × 3), and dried over magnesium sulfate. The solvent was removed under reduced pressure, and the crude product was purified by column chromatography (silica gel, CH_2Cl_2/hexane 1:6) to afford **M4** (3.4 g). Yield: 86%. ^{1}H NMR (ppm, $CDCl_3$): δ 7.04 (d, J = 3.0 Hz, 2H), 6.93 (d, J = 3.0 Hz, 2H), 2.87 (t, J = 7.2 Hz, 4H), 1.75 (m, 4H), 1.42−1.31 (m, 12H), 0.89 (t, J = 7.2 Hz, 6H). ^{13}C NMR (ppm, $CDCl_3$): δ 157.95 (2C), 155.02 (2C), 134.36 (2C), 130.53 (2C), 127.66 (2C), 126.66 (2C), 113.26 (2C), 31.59 (2C), 30.28 (2C), 29.42 (2C), 29.10 (2C), 22.59 (2C), 14.07 (2C). MS (FAB): *m/z* [M^+] 659; calcd *m/z* [M^+] 658.0. Anal. Calcd for $C_{26}H_{30}Br_2N_2S_4$: C, 47.42; H, 4.59; N, 4.25; S, 19.47. Found: C, 47.47; H, 4.31; N, 4.39; S, 19.81.

2,2′-Dibromo-5,5′-bis(bithienyl)-4,4′-dihexyl-2,2′-bithiazole (**M5**). The synthesis of monomer **M5** was followed by the similar procedure as described for monomer **M4**. Compound **9** (1.71 g, 2.57 mmol) was dissolved in chloroform (50 mL) under nitrogen, and then *N*-bromosuccinimide (0.92 g, 5.19 mmol) was added completely. The final solution was purified by column chromatography (silica gel, CH_2Cl_2/hexane 1:3) to yield a red solid (1.94 g). Yield: 92%. ^{1}H NMR (ppm, $CDCl_3$): δ 7.07 (m, 4H), 7.00−6.98 (d, J = 3.9 Hz, 2H), 6.95−6.93 (d, J = 4.5 Hz, 2H), 2.94 (t. J = 7.2 Hz, 4H), 1.82−1.77 (m, 4H), 1.45−1.31 (m, 12H), 0.91−0.87 (m, 6H). ^{13}C NMR (ppm, $CDCl_3$): δ 157.65 (2C), 154.83 (2C), 138.09 (2C), 137.20 (2C), 132.21 (2C), 130.77 (2C), 128.02 (2C), 127.27 (2C), 124.44 (2C), 124.13 (2C), 31.62 (2C), 30.49 (2C), 29.36 (2C), 29.16 (2C), 22.61 (2C), 14.09 (2C). MS (FAB): *m/z* [M^+] 822.0; calcd *m/z* [M^+] 821.9. Anal. Calcd for $C_{34}H_{34}Br_2N_2S_6$: C, 49.63; H, 4.16; N, 3.40; S, 23.38. Found: C, 49.23; H, 4.31; N, 3.20; S, 23.95.

M6. A mixture of compound **10** (2.4 g, 6.1 mmol), compound **11** (6.0 g, 30.5 mmol), and methanol (300 mL) were placed in a 500 mL two-neck round-bottom flask at room temperature. A catalytic amount of potassium *tert*-butoxide in methanol was added into this mixture. After reaction for 24 h, the product was filtered and dried. **M6** was obtained as a red solid (4.1 g) by column chromatography on silica gel eluted with CH_2Cl_2/hexane 1:4. Yield:

Scheme 2. Synthetic Pathways of Bithiazole-Based Monomers M4−M6 and Cyclopentadithiophene

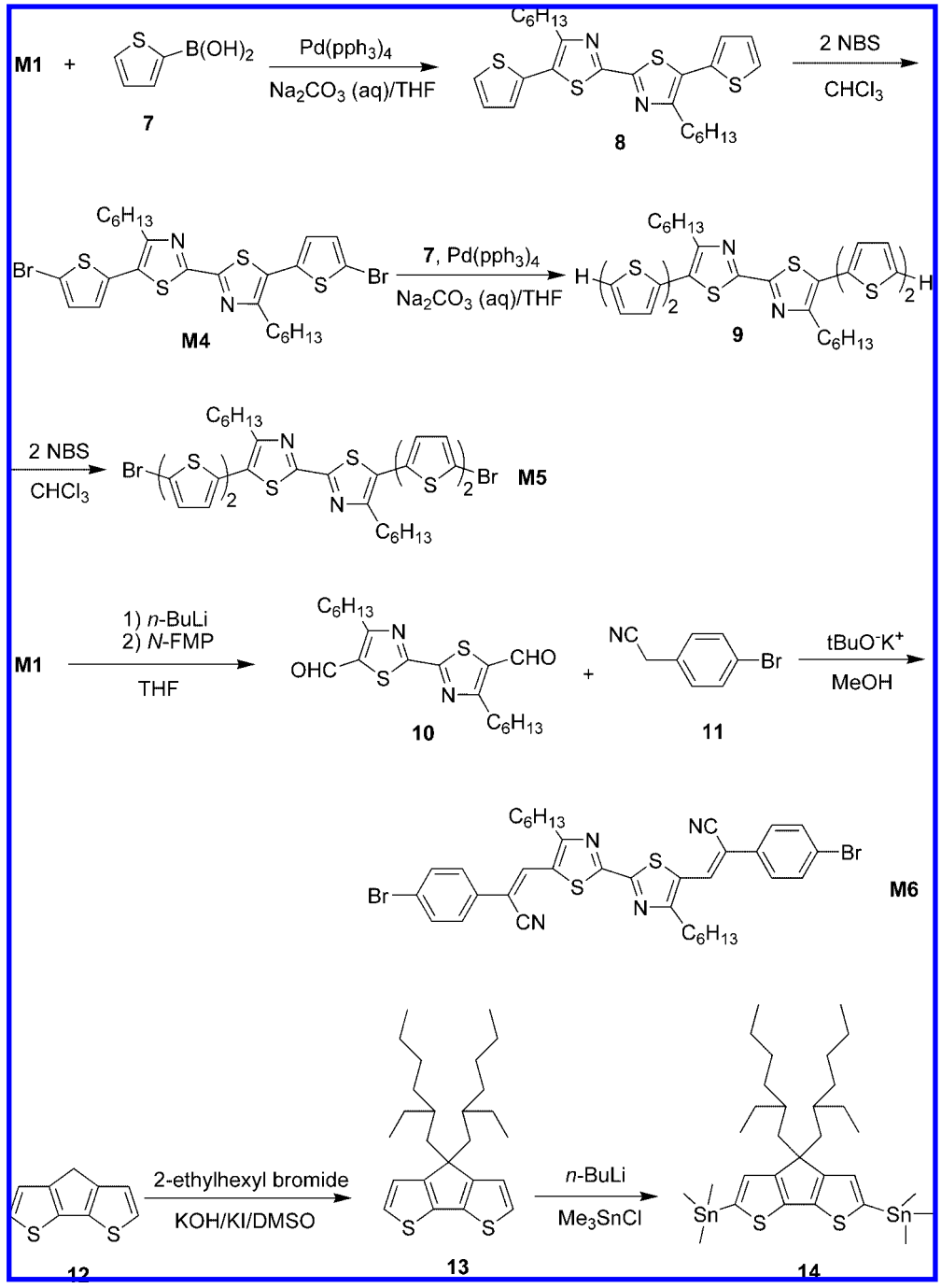

90%. ^{1}H NMR (ppm, $CDCl_3$): δ 7.64 (s, 2H), 7.51−7.39 (m, 8H), 2.93 (t. J = 7.2 Hz, 4H), 1.80 (m, 4H), 1.35 (m, 12H), 0.89 (t. J = 7.2 Hz, 6H). ^{13}C NMR (ppm, $CDCl_3$): δ 164.93 (2C), 160.81 (2C), 132.46 (2C), 132.30 (4C), 130.76 (2C), 129.34 (2C), 127.09 (4C), 123.64 (2C), 117.24 (2C), 109.29 (2C), 31.58 (2C), 30.21 (2C), 29.86 (2C), 29.14 (2C), 22.59 (2C), 14.08 (2C). MS (FAB): m/z [M^+] 749; calcd m/z [M^+] 748.1. Anal. Calcd for $C_{36}H_{36}Br_2N_4S_2$: C, 57.76; H, 4.85; N, 7.48; S, 8.57. Found: C, 57.62; H, 4.72; N, 7.60; S, 9.04.

General Procedure for the Synthesis of Copolymers **P1**−**P6**. [6c,20] The synthetic route of copolymers is shown in Scheme 3. All polymerization steps were carried out through the palladium(0)-catalyzed Stille coupling reactions. Into 50 mL of two-neck flask, 1 equiv of dibromo monomers (**M1**-**M6**) and 1 equiv of 4,4-bis(2-ethylhexyl)-2,6-bis(trimethylstannanyl)-4*H*-cyclopenta[2,1-*b*:3,4-*b*′]dithiophene (**14**) were added in anhydrous toluene and deoxygenated with nitrogen for 30 min. The Pd(0) complex, i.e., tetrakis(triphenylphosphine)palladium (1 mol %), was transferred into the mixture in a dry environment. The reaction mixture was stirred at 110 °C for 4−5 days, and then an excess amount of 2-bromothiophene was added to end-cap the trimethylstannyl groups for 4 h. The reaction mixture was cooled to 40 °C and added slowly into a vigorously stirred mixture of methanol/acetone (3:1). The polymers were collected by filtration and reprecipitation from methanol. The crude polymers were further purified by washing with acetone and EA for 2 days in a Soxhlet apparatus to remove oligomers and catalyst residues, respectively.

P1. Following the general polymerization procedure, compound **14** (1.0 mmol), **M1** (1.0 mmol), and toluene (8 mL) were used in this polymerization, and the polymer was obtained as a dark red powder. Yield: 46%. ^{1}H NMR (ppm, $CDCl_3$): δ 7.07 (br, s, 2H), 2.98 (br, s, 4H), 1.83 (br, m, 8H), 1.46−1.02 (br, m, 12H), 0.96−0.91 (br, m, 22H), 0.75−0.61 (br, m, 14H). Anal.

Scheme 3. Synthetic Routes of Copolymers P1−P6

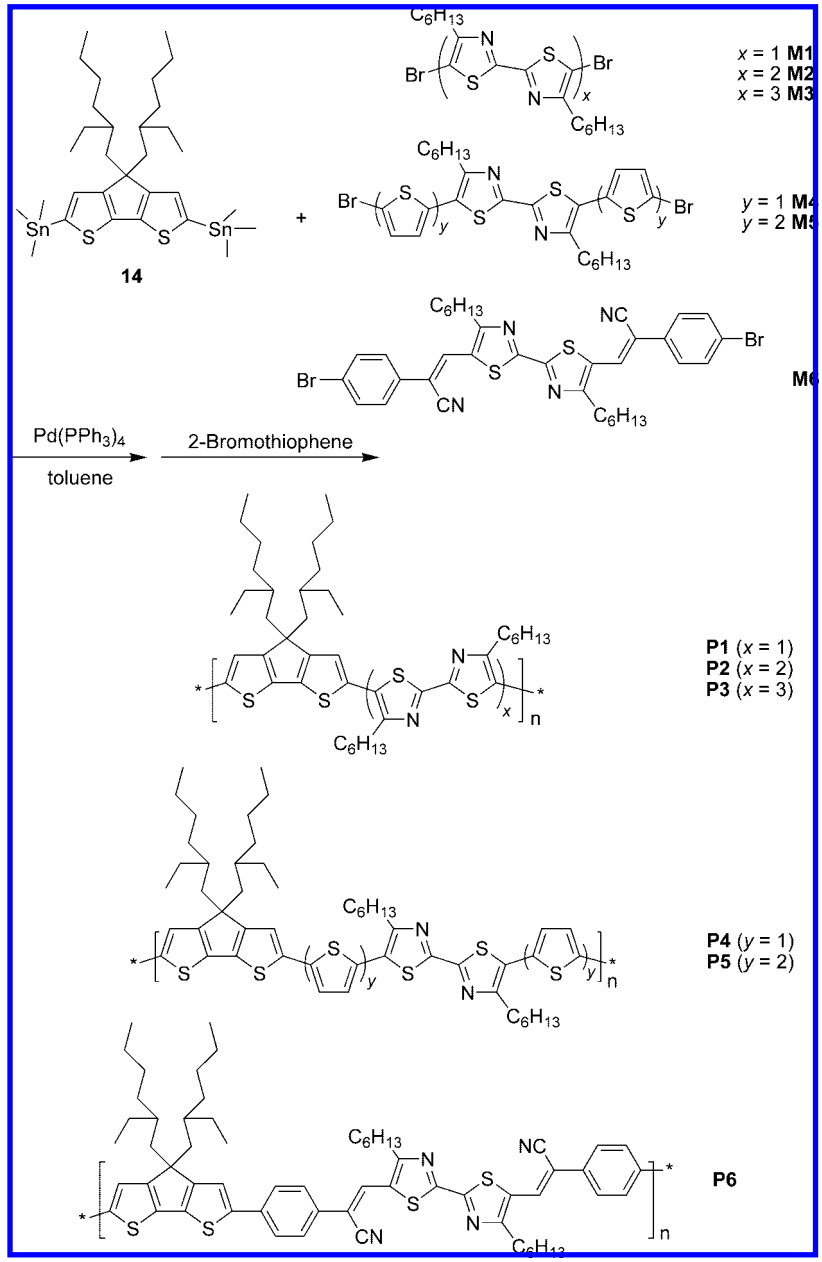

Calcd for $C_{43}H_{62}N_2S_4$: C, 70.25; H, 8.50; N, 3.81. Found: C, 68.77; H, 8.25; N, 3.59.

P2. Following the general polymerization procedure, compound **14** (0.96 mmol), **M2** (0.96 mmol), and toluene (8 mL) were used in this polymerization, and the polymer was obtained as a black powder. Yield: 58%. ^{1}H NMR (ppm, $CDCl_3$): δ 7.09 (br, s, 2H), 2.99 (br, s, 4H), 2.74 (br, s, 4H), 1.74 (br, m, 12H), 1.45−1.29 (br, m, 24H), 1.03−0.85 (br, m, 28H), 0.77−0.61 (br, m, 14H). Anal. Calcd for $C_{61}H_{88}N_4S_6$: C, 68.49; H, 8.29; N, 5.24. Found: C, 67.26; H, 7.24; N, 5.10.

P3. Following the general polymerization procedure, compound **14** (0.72 mmol), **M3** (0.72 mmol), and toluene (6 mL) were used in this polymerization, and the polymer was obtained as a dark black powder. Yield: 65%. ^{1}H NMR (ppm, $CDCl_3$): δ 7.09 (br, s, 2H), 2.98 (br, s, 4H), 2.75 (br, 2, 8H), 1.74 (br, m, 16H), 1.29 (br, m, 36H), 1.03−0.87 (br, m, 34H), 0.76−0.62 (br, m, 14H). Anal. Calcd for $C_{79}H_{114}N_6S_8$: C, 67.57; H, 8.18; N, 5.98. Found: C, 65.94; H, 7.77; N, 5.94.

P4. Following the general polymerization procedure, compound **14** (0.68 mmol), **M4** (0.68 mmol), and toluene (6 mL) were used in this polymerization, and the polymer was obtained as a dark black powder. Yield: 61%. ^{1}H NMR (ppm, $CDCl_3$): δ 7.11−7.07 (br, m, 6H), 2.99 (br, s, 4H), 1.83 (br, m, 8H), 1.46−1.37 (br, m, 12H), 1.03−0.92 (br, m, 22H), 0.77−0.61 (br, m, 14H). Anal. Calcd for $C_{51}H_{66}N_2S_6$: C, 68.10; H, 7.40; N, 3.11. Found: C, 67.31; H, 7.21; N, 3.34.

P5. Following the general polymerization procedure, compound **14** (0.74 mmol), **M5** (0.74 mmol), and toluene (6 mL) were used in this polymerization, and the polymer was obtained as a dark black powder. Yield: 58%. ^{1}H NMR (ppm, $CDCl_3$): δ 7.11−6.97 (br, m, 10H), 2.94 (br, s, 4H), 1.79 (br, m, 8H), 1.45−1.37 (br, m, 12H), 0.91−0.87 (br, m, 22H), 0.77−0.61 (br, m, 14H). Anal. Calcd for $C_{59}H_{70}N_2S_8$: C, 66.62; H, 6.63; N, 2.63. Found: C, 65.69; H, 7.04; N, 2.55.

P6. Following the general polymerization procedure, compound **14** (0.96 mmol), **M6** (0.96 mmol), and toluene (12 mL) were used in this polymerization, and the polymer was obtained as a dark black powder. Yield: 15%. ^{1}H NMR (ppm, $CDCl_3$): δ 7.71−7.42 (br, m, 12H), 2.96 (br, s, 4H), 1.90 (br, m, 8H), 1.49−1.35 (br, m, 12H), 1.00−0.92 (br, m, 22H), 0.73−0.60

Table 1. Molecular Weights, Yields, and Thermal Data of Copolymers P1−P6

polymer	M_n[a] (×10³)	M_w[a] (×10³)	PDI	yield (%)	transition temperature (°C) T_g[b]	T_m[b]	T_c[b]	T_d[c]
P1	15.1	20.3	1.34	46	n.d.[d]	n.d.[d]	n.d.[d]	363
P2	38.0	52.2	1.37	58	130	n.d.[d]	n.d.[d]	395
P3	42.1	70.0	1.66	65	161	n.d.[d]	n.d.[d]	398
P4	17.7	32.0	1.81	61	168	237	207	396
P5	9.5	14.0	1.47	58	123	256	244	398
P6	5.1	5.5	1.08	15	n.d.[d]	n.d.[d]	n.d.[d]	377

[a] Molecular weights and polydispersity were measured by GPC, using THF as an eluent, polystyrene as a standard. M_n, number average molecular weight. M_w, weight average molecular weight. [b] Glass transition temperature, melting temperature, and crystalline temperature (°C) were measured by DSC at a heating rate of 10 °C/min. [c] Temperature (°C) at 5% weight loss measured by TGA at a heating rate of 20 °C/min under nitrogen. [d] No noticeable transition temperature was observed.

(br, m, 14H). Anal. Calcd for $C_{61}H_{72}N_4S_4$: C, 74.04; H, 7.33; N, 5.66. Found: C, 72.53; H, 7.79; N, 5.21.

Results and Discussion

Synthesis and Chemical Characterization. Six new donor−acceptor bithiazole-based (BT) monomers **M1**−**M6** were prepared from 4,4′-dihexyl-2,2′-bithiazole (**1**)[14a] via Stille and Suzuki coupling reactions. By insertion of phenylene and cyanovinylene functionalities to BT units, oligo(bithiazole)s **M1**−**M3**, and bithiazole−oligo(thiophene)s **M4**−**M6** were obtained correspondingly, and their synthetic routes are outlined in Schemes 1 and 2. Monomers **M1**−**M6** and compound **14** were satisfactorily characterized by ^{1}H NMR, ^{13}C NMR, MS spectroscopy, and elemental analyses. As shown in Scheme 3, further Stille coupling of bis-stannane **14** with monomers **M1**−**M6** successfully resulted in the well-defined CPDT−BT copolymers **P1**−**P6**.[6c,20] The attached pendants of two 2-ethylhexyl side chains on CPDT units and one long hexyl chain on bithiazole units were crucial to enhance the solubilities and the solution processabilities/tractabilities of these copolymers. All the copolymers were completely soluble in organic solvents such as chloroform, THF, and chlorobenzene at room temperature, except that copolymers **P5** and **P6** were only completely soluble in high boiling point solvents (e.g., chlorobenzene). The less solubilities of copolymers **P5** and **P6** were likely owing to the higher rigidities of the polymer main chains caused by the larger number of thiophene units and rigid electron-withdrawing cyano groups.

The yields and molecular weights of copolymers **P1**−**P6** determined by GPC against polystyrene standards in THF are summarized in Table 1. After washing final products in Soxhlet apparatus, the yields of 15−65% for **P1**−**P6** were obtained. The copolymers have the number molecular weights (M_n) of 5100 to 42100 with the polydispersity index (PDI) values ranging 1.08−1.81. The molecular weights of copolymers **P5**−**P6** were relatively smaller than the other copolymers, which were likely due to the lower solubilities originated from the rigid thiophene and cyano groups. The thermal stabilities and phase transition temperatures of copolymers **P1**−**P6**, including 5% weight loss temperatures (T_d), glass transition temperatures (T_g), melting temperatures (T_m), and crystallization temperatures (T_c) characterized by TGA and DSC are summarized in Table 1. All copolymers were thermally stable up to 363−398 °C upon heating and showed T_g values over 120 °C, except that the phase transition temperatures of **P1** and **P6** were not observed by DSC. The detectable melting temperatures (T_m) and crystallization temperatures (T_c) of copolymers **P4** and **P5** suggested the higher ordering capabilities of **P4** and **P5** for their potential applications in organic solar cells, since the formation of phase-separated ordered nanostructures in the photovoltaic layer was desirable for charge transport and separation.[21,22]

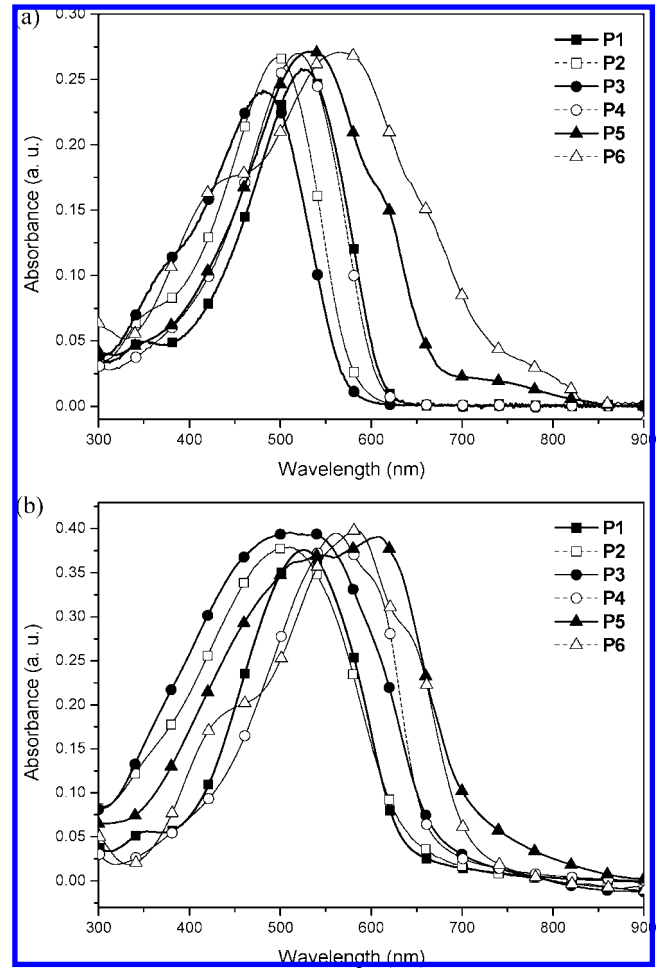

Figure 1. Optical absorption spectra of D−A copolymers **P1**−**P6** (a) in chlorobenzene solutions, and (b) in solid films (spin-coated from chlorobenzene solutions).

Table 2. Photophysical Data and Optical Bandgap of Copolymers P1−P6

polymer	λ_{max}, UV (fwhm)[a] solution (nm)[b]	film (nm)[b]	E_g^{opt} (eV)[c]
P1	525 (130)	527 (150)	1.94
P2	500 (133)	516 (205)	1.90
P3	482 (143)	511 (260)	1.83
P4	523 (130)	560, 607[d]	1.84
P5	536, 613[d]	544,[d] 616	1.70
P6	426,[d] 570, 645[d]	443,[d] 587, 650[d]	1.71

[a] Fwhm = Full width at half-maximum. [b] Obtained or spin-coated from chlorobenzene solutions. [c] Estimated from the onset wavelengths of UV−vis spectra in solid films. [d] Shoulder peak.

Optical properties. The optical absorption spectra of copolymers **P1**−**P6** in chlorobenzene solutions (10^{-6} M) and solid films are shown in Figure 1. The photophysical properties of the D−A copolymers (**P1**−**P6**) based on CPDT−BT units are illustrated in Table 2. As expected, by tuning the numbers of the conjugated heterocyclic rings and electron donor−acceptor compositions, the conjugation lengths of the copolymers will be affected, which will also influence the absorption spectra of **P1**−**P6** effectively (in both solutions and solid films). For instance, due to the presence of a more extended and delocalized π-electron system by increasing the number of the donor thiophene (Th) ring, an obvious red-shifted absorption of copolymer **P5** was observed compared with that of copolymer **P4** in both solutions and solid films. Furthermore, copolymer **P6** containing electron-accepting cyano groups showed the longest absorption wavelength among all copolymers in solu-

tions. However, the numbers of BT acceptor units in copolymers **P1**−**P3** affected the absorption maxima in solutions and solid films by different ways. Surprisingly, a blue-shifted absorption in solutions was observed by increasing the number of BT units in solutions of **P1**−**P3**, which might be due to the twist of polymer main chains by the BT units with alkyl side-chains. Nevertheless, due to the enlarged full width at half-maximum (fwhm) values from **P1** to **P3**, a blue-shifted absorption in solid films of **P1**−**P3** was observed; but their optical band gaps (in solid films) had been reduced from 1.94 eV of **P1** to 1.83 eV of **P3**. Even though the numbers of the conjugated rings in both **P2** and **P4** or both **P3** and **P5** are the same, the electron donor (Th) and acceptor (BT) units still have some influences on copolymers **P2**−**P5**. Compared with copolymers **P2** and **P3**, the corresponding **P4** and **P5** had 23 nm (44 nm) and 54 nm (105 nm) of redder absorption maxima in solutions (in solid films), respectively, which implied that the electron donor (Th) units had more contributions to enlarge the conjugation lengths in the copolymers than the BT units. Similar changes of UV−vis spectra were found in rigid π-conjugated polymers with an intramolecular charge transfer (ICT) interaction between electron donor and acceptor moieties.[14b,23]

Interestingly, by increasing the numbers of the conjugated heterocyclic rings in the donor−acceptor systems, the gradually enhanced red-shifted absorption (from solutions to solid films) in **P1**−**P5** were likely due to their longer conjugated organization, which led to higher aggregation forms of these copolymer chains in solid films in contrast to those in solutions. The optical band gaps (E_g^{opt}) of the copolymers in solid films, which were determined by the cutoff wavelengths of the optical absorptions, were in the range of 1.70−1.94 eV (Table 2). As a result, the electron donor Th rings in combination with the electron acceptor BT rings[12,14b] or cyano groups[24,25] presented a more extended π-conjugated system through the rigid main-chains and electron D−A chromophores, where the optical band gaps of **P1**−**P6** were gradually lowered from **P1** with the largest value of 1.94 eV to **P5** with the narrowest value of 1.70 eV (0.24 eV lower than **P1**).

As shown in Figure S1 (see Supporting Information), the intensities of PL emission spectra in solid films of **P4**−**P6** were more dramatically quenched than those in **P1**−**P3**, which suggested that the more efficient photoinduced charge transfer was likely due to the presence of the stronger donor−acceptor effects. Thus, this charge transfer might be satisfactorily rapid to complete the radiative recombination of excitons.[26] The appropriate photophysical properties of these copolymers in solid films, including broad and strong optical absorptions as well as effective charge transfers, proposed their potential applications for photovoltaic cells described below.

Electrochemical Characterization. The electrochemical results are shown in Figure 2 and the data are summarized in Table 3. The formal oxidation potentials were in the range of 0.79−1.24 V (the first peaks) for **P1**−**P6**, 0.98−1.42 V (the second peaks) for **P2**−**P5**, and 1.34−1.68 V (the third peaks) for **P3**−**P5**. In addition, the formal reduction potentials were in the range of −(0.88−1.05) V (the first peaks) and −(1.13−1.77) V (the second peaks) for **P1**−**P6**, respectively. Both reversible oxidation and reduction were found in **P1**, whereas irreversible oxidation and partially reversible reduction were observed in **P2** and **P3**. It suggested that **P1** containing electron-donating CPDT and electron-accepting BT moieties was closer to be both p-type and n-type materials. As the electron-accepting character of BT moieties increased in **P2** and **P3**, they were found to be suitable as n-type materials than p-type materials. Besides, **P4**, **P5**, and **P6** all exhibited partially reversible oxidation and reduction behavior as evident from the areas and close proximity of the anodic and cathodic scans,

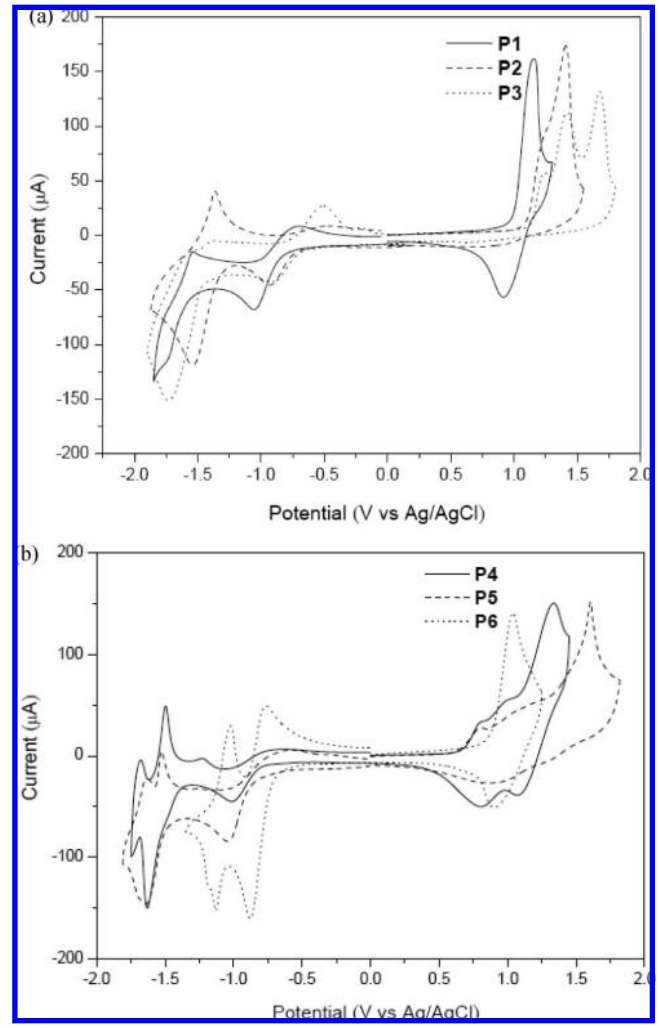

Figure 2. Cyclic voltammograms of D−A copolymers (a) **P1**−**P3** and (b) **P4**−**P6** (at a scan rate of 100 mV/s in solid films).

which were a good sign for high structural stability in the charged state.

The moderate onset oxidation potentials and onset reduction potentials of **P1**−**P6** were observed between 0.64−1.15 V and −(0.67−0.87) V, respectively, from which the HOMO levels of 5.04−5.55 eV and LUMO levels of 3.53−3.73 eV for all copolymers were calculated according to the following equation:[16b] $E_{HOMO}/E_{LUMO} = [-(E_{onset\ (vs\ Ag/AgCl)} - E_{1/2}\ (ferrocene)+4.8)]$ eV, where 4.8 eV was the energy level of ferrocene below the vacuum level. It was worthwhile to note that the oxidation potentials of copolymers **P1**−**P6** were significantly varied when different numbers of Th donor units and BT/cyano acceptor moieties were incorporated into the molecular structures. Interestingly, the oxidation potentials of **P1**−**P3** and **P6** were ca. 0.2 V higher than those of **P4**−**P5**, thus indicating higher oxidation stability for **P1**−**P3** and **P6**. The noticeably higher oxidation potentials **P1**−**P3** and **P6** can be explained by that the resulting conjugated copolymers were more electron-deficient due to the nitrogen atoms in their planar π-conjugated systems. Oppositely, in contrast to **P4**, the oxidation potential of **P5** was reduced by the extension of Th rings, and thus **P5** showed a lower oxidation potential (0.64 V) due to the longer Th ring. On the other hand, the LUMO energy level of the donor (polymer) has to be positioned above the LUMO energy level of the acceptor (PCBM) by at least 0.3 eV, so the exciton binding energy of polymer could be overcome and result in efficient electron transfer from donor to acceptor.[16b] Hence, the electrochemical reduction potentials of copolymers **P1**−**P6**

Table 3. Electrochemical Potentials, Energy Levels, and Band Gaps of Copolymers P1−P6[a]

	oxidation potential[a] (V)		reduction potential (V)		energy level[d] (eV)		band gap[e] (eV)
polymer	$E_{ox/onset}$[b]	$E_{ox/o}$[c]	$E_{red/onset}$[b]	$E_{red/o}$[c]	E_{HOMO}	E_{LUMO}	E_g
P1	1.00	1.16	−0.83	−1.05	−5.40	−3.57	1.83
			−1.57	−1.77			
P2	1.11	1.22	−0.71	−0.89	−5.51	−3.69	1.82
		1.42	−1.36	−1.52			
P3	1.15	1.24	−0.67	−0.88	−5.55	−3.73	1.82
		1.42	−1.48	−1.73			
		1.68					
P4	0.67	0.80	−0.85	−1.01	−5.07	−3.55	1.52
		0.98	−1.49	−1.63			
		1.34					
P5	0.64	0.79	−0.87	−1.03	−5.04	−3.53	1.51
		1.15	−1.51	−1.64			
		1.60					
P6	0.88	1.04	−0.73	−0.88	−5.28	−3.67	1.61
			−1.09	−1.13			

[a] Reduction and oxidation potentials measured by cyclic voltammetry in solid films. [b] Onset oxidation and reduction potentials. [c] Formal oxidation and reduction potentials. [d] Estimated from the onset potentials using empirical equations: $E_{HOMO}/E_{LUMO} = [-(E_{onset\ (vs\ Ag/AgCl)} - E_{1/2}\ (ferrocene) + 4.8)]$ eV, where 4.8 eV is the energy level of ferrocene below the vacuum level. [e] Band gaps measured by cyclic voltammograms.

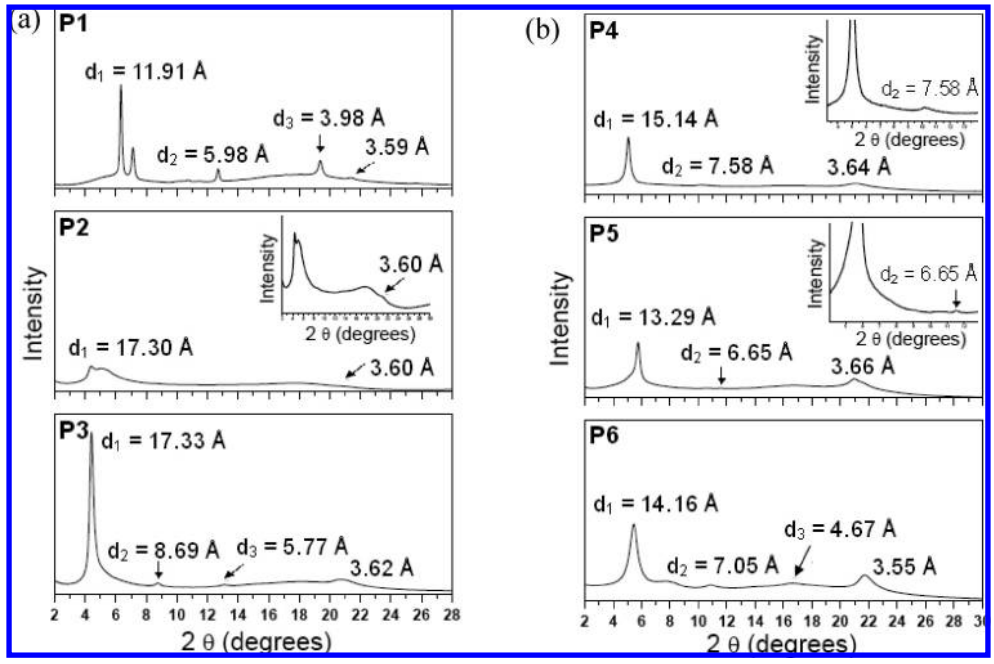

Figure 3. X-ray diffraction patterns of copolymers **P1−P6** in powder solids. The sharp diffraction peaks indicated that copolymers formed ordered structures in the solid state.

showed similar LUMO energy levels at ca. 3.53−3.73 eV, which represented high electron affinity to make these copolymers suitable donors to inject and transport electrons to PCBM acceptor (with 0.57−0.77 eV LUMO offsets regarding the LUMO level of PCBM at 4.3 eV[16]) for the bulk heterojunction polymer solar cell devices.[27] The differences between the band gap values directly measured by CV (E_g^{ec} between 1.51 and 1.83 eV) and the optical band gap values obtained from UV−vis spectra (E_g^{opt} between 1.70 and 1.94 eV) lied within an acceptable range of errors.

X-ray Diffraction. As shown in Figure 3, powder X-ray diffraction (XRD) patterns of copolymers **P1−P6** were acquired to investigate the molecular organization and morphological change after the thermal treatment of ca. 150 °C for 5 min. Interestingly, except **P2**, the annealed copolymers **P1** and **P3−P6** exhibited several strong diffraction peaks with high crystalline patterns, similar to the thiazole-[12a−e,13] and thiophene-based polymers.[4b,6c,28] Distinct primary diffraction peaks at $2\theta = 6.3°$, 4.3°, 4.3°, 5.1°, 5.7°, and 5.4° (small-angle region), corresponding to the d_1-spacing values of 11.9, 17.3, 17.3, 15.1, 13.3, and 14.2 Å for copolymers **P1−P6**, were assigned to the interchain spacing between polymer main chains, where the alkyl substituents were segregated as reported for similar π-conjugated polymers with long side chains.[4b,6c,12a−e,13,28] The second-order diffraction peaks for **P1** and **P3−P6** as well as the third-order diffraction peaks for **P1**, **P3,** and **P6** were clearly observed at d_1/n Å ($n = 2-3$), respectively, which implied a highly organized assembly of these π-conjugated copolymers. Planar polymer molecules with side chains might prefer the face-to-face parallel packing.[13b] Some reasonable packing modes of these copolymers in view of van der Waals contacts are depicted in Figure S2 (see Supporting Information). The distances between the segregation of the polymer main chains accounted for the interchain d_1 spacings. The distances between top and bottom layers of the backbones accounted for the $\pi-\pi$ stacking at wide-angle d spacings. The regioregular $\pi-\pi$ stacking distances of the backbones in **P1−P6** were in the range of wide-angle X-ray diffraction (XRD) at 3.55−3.66 Å, which were somewhat smaller than that (ca. 3.80 Å) observed in HT-P3RTh[29] with a similar stacked structure. It suggested that the

Table 4. Photovoltaic Properties of PSC Devices Containing an Active Layer of P1−P6:PCBM = 1:1 (w/w) with the Configuration of ITO/PEDOT:PSS/Polymer:PCBM/Ca/Al[a]

active layer[b] (polymer:PCBM = 1:1)	V_{oc} (V)	I_{sc} (mA/cm^2)	FF (%)	PCE (%)	mobility (cm^2 V^{-1} s^{-1})	max. EQE (%)
P1	0.730	6.34	53.0	2.45	5.4×10^{-4}	50
P2	0.777	5.26	51.9	2.12	5.6×10^{-4}	40
P3	0.822	4.43	49.3	1.78	4.7×10^{-4}	36
P4	0.683	7.70	53.0	2.79	5.2×10^{-4}	60
P5	0.729	3.03	36.1	0.80	3.9×10^{-4}	28
P6	0.630	2.68	32.0	0.54	3.3×10^{-4}	28

[a] Measured under 100 mW/cm^2 of AM 1.5 irradiation. [b] Active layer with the weight ratio of **P1**−**P6**:PCBM = 1:1.

π-conjugated polymers containing thiazole units had a stronger tendency to form the face-to-face stacking than those containing thiophene units.[13]

In bithiazole-based copolymers **P2** and **P3**, the larger d_1 spacing of 17.3 Å was presumed to adopt the possible end-to-end packing motifs and π-stacking structures, because the number density of the alkyl groups was similar to that of HT-P3RTh (ca. 17.7 Å),[13a] as illustrated in Figure S2(b). Interestingly, **P1** and **P4**-**P6** showed smaller d_1 spacing values of 11.9−15.1 Å than **P2** and **P3**, which suggested that the packings of these copolymer chains were likely interdigitated in the lamellar sheets, as shown in Figure S2(a). The number densities of the alkyl groups in these copolymers were not as high as those of **P2** and **P3**, and furthermore the nonsubstituted thiophene rings or arylcyanovinyl units provided a sufficient space to facilitate the side-chain interdigitation. Based on the observation, it could be assumed that these characters of **P1**−**P6** formed highly crystalline diffraction patterns, indicating good $\pi-\pi$ stacking of coplanar π-conjugated backbones with very promising electro-optical properties. Overall, the charge carrier mobilities of PSC devices were substantially improved by increasing the crystallinities and intermolecular stacking degrees in solid films.

Organic Photovoltaic Cell Properties. According to the previously described physical properties of **P1**−**P6**, these coplanar semiconducting copolymers **P1**−**P6** are suitable for PSC applications. To investigate the potential use of copolymers **P1**−**P6** in PSCs, bulk heterojunction PSC devices with a configuration of ITO/PEDOT:PSS/**P1**−**P6**:PCBM (1:1 w/w)/Ca/Al were fabricated from an active layer where copolymers **P1**−**P6** were blended with a complementary fullerene-based electron acceptor (PCBM) in a weight ratio of 1:1 (w/w) initially (and later followed with various weight ratios for the optimum copolymer). The photovoltaic properties of PSC devices containing copolymers **P1**−**P6**:PCBM (1:1 w/w) are listed in Table 4. Parts a and b of Figure 4 illustrate $I-V$ curves and EQE values, respectively, for PSC devices containing copolymers **P1**−**P6**:PCBM (1:1 w/w) under monochromatic illumination, where EQE is displayed as a function of wavelength. Due to the minor variations in open circuit voltage (V_{oc}) values (0.822−0.630 V) in **P1**−**P6**, Figure 4a demonstrates the sequence of the best power conversion efficiency (PCE) values for **P4**, **P1**, and **P2** according to their short circuit current density (I_{sc}) values of 7.70, 6.34, and 5.26 mA/cm^2, respectively. As shown in Figure 4b, broader EQE curves for **P4**, **P1**, and **P2** covered almost the entire visible spectrum from 350 to 650 nm with the maximum EQE values of 60%, 50%, and 40%, respectively, which also explained for their high power conversion efficiency (PCE) values over 2.12%. Among these PSC devices containing copolymers **P1**−**P6**, the best performance was the PSC device fabricated by **P4**:PCBM (1:1 w/w) which reached an AM 1.5G power conversion efficiency (PCE) of 2.79%, with a short circuit current density (I_{sc}) of 7.70 mA/cm^2, an open circuit voltage (V_{oc}) of 0.683 V, and a fill factor (FF) of 0.53.

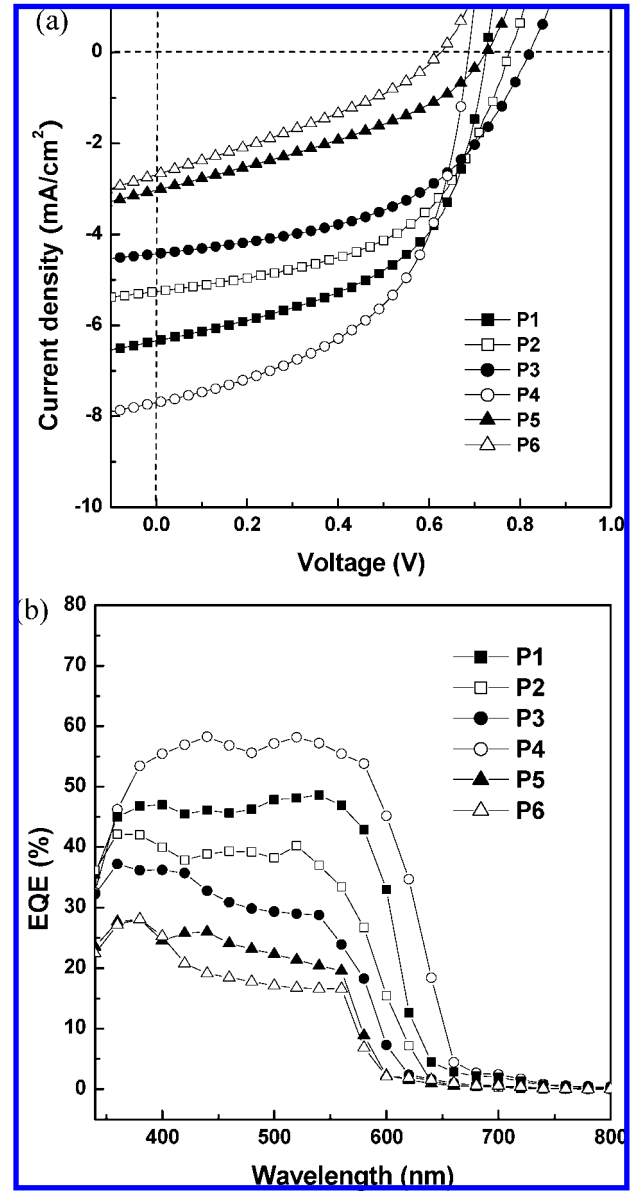

Figure 4. (a) $I-V$ curves (under simulated AM 1.5 solar irradiation) and (b) EQE wavelength dependencies of PSC devices with an active layer of blended copolymers **P1**−**P6**:PCBM (1:1 w/w).

Due to the requirements of higher charge mobilities and better absorptions of polymers in PSC devices,[30] the hole mobility values of copolymers **P1**−**P6** were (see Table 4) estimated from eq 1

$$J = 9\varepsilon_0\varepsilon_r\mu V^2/8L^3 \quad (1)$$

via space-charge limit current (SCLC) by fabricating a hole-only device,[17] where $\varepsilon_0\varepsilon_r$ is the permittivity of the polymer, μ is the carrier mobility, L is the device thickness. Ideally, I_{sc} was

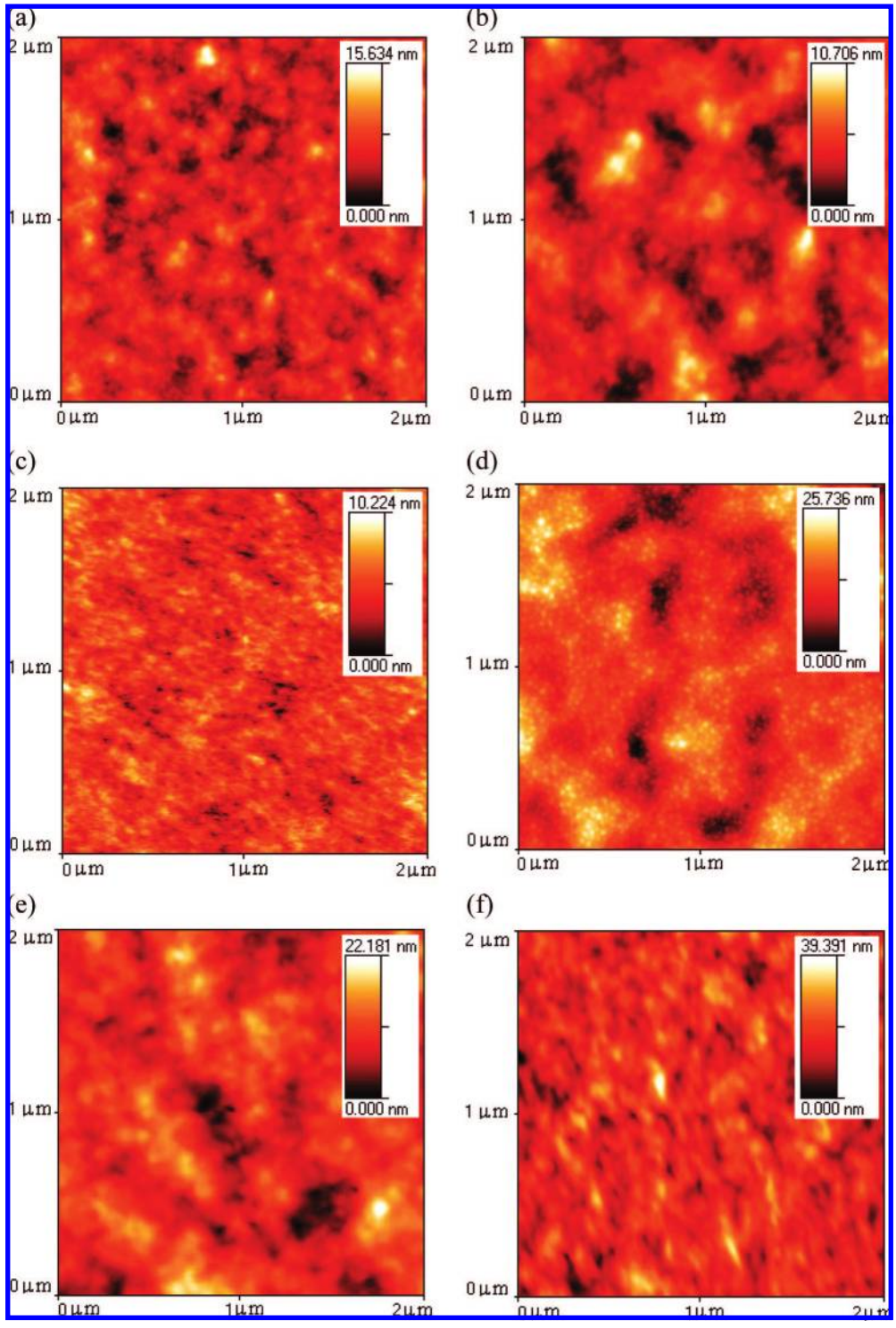

Figure 5. AFM images for solid films of blended copolymers (a) **P1**, (b) **P2**, (c) **P3**, (d) **P4**, (e) **P5**, and (f) **P6** with PCBM (1:1 w/w) as-cast from DCB solutions.

determined by the product of the photoinduced charge carrier density and the charge carrier mobility within the organic semiconductors.[31a] Surprisingly, the hole mobilities of copolymers **P5**−**P6** were not as high as those of copolymers **P1**−**P4**, which was probably due to the lower molecular weights and worse soubilities resulting in inferior film-forming qualities, even though their optical band gaps were smaller than the other copolymers (**P1**−**P4**). Thus, due to the relatively lower hole mobilities and less light-harvesting capabilities at the longer absorption wavelength ranges of **P3**, **P5**, and **P6**, their PSC devices showed lower photocurrent values of 4.43, 3.03, and 2.68 mA/cm^2, respectively, in comparison with those containing **P1**, **P2**, and **P4**. This phenomenon of lower photocurrents further explained the worse EQE values and narrower absorption wavelength regions in the PSC devices containing copolymers **P3**, **P5**, and **P6**, where the EQE values of the visible spectra from 350 to 600 nm were only below 40%. Thus, not only optical properties but also charge transporting properties could be tuned by changing the lengths of oligothienyl and bithiazole-based main-chains. Comparing the FF values in **P1**−**P4** (excluding **P5**−**P6** due to their poor soubilities), the highest values of 53% in PSC devices containing copolymers **P1** and **P4** were obtained likely due to the more densely packed lamellar sheets in **P1** and **P4** (with smaller d_1 spacing values of 11.9

and 15.1 Å resulting from highly ordered structural packings) than **P2** and **P3** with a longer d_1 spacing value of 17.3 Å), as proven by XRD patterns previously.

The V_{oc} values covered a rather wide range among the PSC devices containing copolymers **P1**−**P6**, which were related to the differences of energy levels between the HOMO levels of the polymers and the LUMO levels of the acceptors.[31] Therefore, the PSC devices containing copolymers **P1**, **P2**, and **P3** (with HOMO energy levels of −5.40, −5.51, and −5.55 eV, respectively) showed slight increases of V_{oc} values (0.730, 0.777, and 0.822 V, respectively), which indicated that the insertion of more bithiazole units had some influence on the relationship between the HOMO levels of copolymers and the V_{oc} values of PSC devices. Moreover, followed by increasing the HOMO level of copolymer **P4** (from −5.40 to −5.07 V), the V_{oc} value of the PSC device containing **P4** was ca. 0.05 V lower than that containing **P1**, which was due to the insertion of the strong electron-donating thiophene moieties in the molecular structure of **P4**.

The AFM topographies of polymer blends (**P1**−**P6**:PCBM=1:1 w/w) were investigated by the casting films of DCB solutions as shown in Figure 5, where the images were obtained in a surface area of 2 × 2 μm^2 by the tapping mode. The phase image of blended copolymer **P4** showed coarse chain-like features across the surface, which were attributed to the domains of the highly stacked polymer chains of **P4**. In comparison with blended copolymers **P1**−**P3**, the solid film of blended copolymer **P4** revealed a rather uneven surface with a root-mean-square (rms) roughness of 7.3 nm. The rougher surface of blended copolymer **P4** was caused by the better self-assembled stacking between the bithiazole and thiophene units, which enhanced both hole mobility and photocurrent.[4a] Furthermore, the solid film of blended copolymer **P1** showed the moderate rough surface with a rms roughness of 5.2 nm. However, increasing the numbers of bithiazole units with alkyl side-chains in **P2** and **P3**, the surfaces of polymer blends (**P2** and **P3**) showed rms roughnesses of 3.3 and 2.1 nm, respectively. The smoother surfaces of blended copolymers **P2** and **P3** compared with that of blended copolymer **P1** indicated that more side chains of copolymers **P2** and **P3** would disrupt the polymer crystallization in the polymer blends and led to lower photocurrents. It is worthy to mention that the solid films of blended copolymers **P5** and **P6** showed rather rough surfaces, but the large values of rms roughnesses (6.9 and 9.3 nm) were contributed from the aggregation of polymer chains due to their poor solubilities, which reduced the interfaces between donor (copolymers) and acceptor (PCBM) significantly. Owing to the unfavorable morphologies for charge transport offered by poor solubilities, the PSC devices based on **P5** and **P6** gave relatively low current densities (I_{sc}) as shown in Table 4. Therefore, excluding **P5** and **P6**, the blended copolymers (**P1**−**P4**:PCBM=1:1 w/w) have the same order of PCE values as those of root-mean-square (rms) roughnesses in AFM, i.e., **P4** (7.3 nm) > **P1** (5.2 nm) > **P2** (3.3 nm) > **P3** (2.1 nm).

Since the best performance of PSC devices fabricated by polymer blends **P1**−**P6**:PCBM (1:1 w/w) was made of **P4**, current−voltage characteristics of PSC devices as a function of blended copolymer **P4**:PCBM in various weight compositions are shown in Figure 6 and Table 5. The optimum photovoltaic performance with the maximum PCE value of 3.04% (V_{oc} = 0.70 V, I_{sc} = 8.00 mA/cm^2, FF = 53.7%) was obtained in the PSC device having a weight ratio of **P4**:PCBM=1:2. Using lower weight ratios of PCBM in blended copolymers **P4**:PCBM (**P4**:PCBM=1:0.5 and 1:1 w/w) led to reductions in the I_{sc} values due to the inefficient charge separation and electron transporting properties, resulting in the lower PCE results.[30b] However, loading larger weight ratios of PCBM in blended copolymers **P4**:PCBM (1:3 and 1:4 w/w) also reduced the I_{sc} and PCE values, which could be probably attributed to the increased aggregation of PCBM so as to influence the separation of charges. Furthermore, an unbalanced charge transporting property was introduced due to the large PCBM ratio. Hence, both I_{sc} and PCE values decreased with larger PCBM molar ratios of 1:3 and 1:4 (w/w) because of the two reasons described here.[32] Therefore, the most efficient PSC device with the maximum PCE value of 3.04% was established by the blended copolymer **P4** with a weight ratio of **P4**/PCBM = 1:2 in this report, which has a similar result as the PSC devices containing thiophene-based polymers.[11b,33]

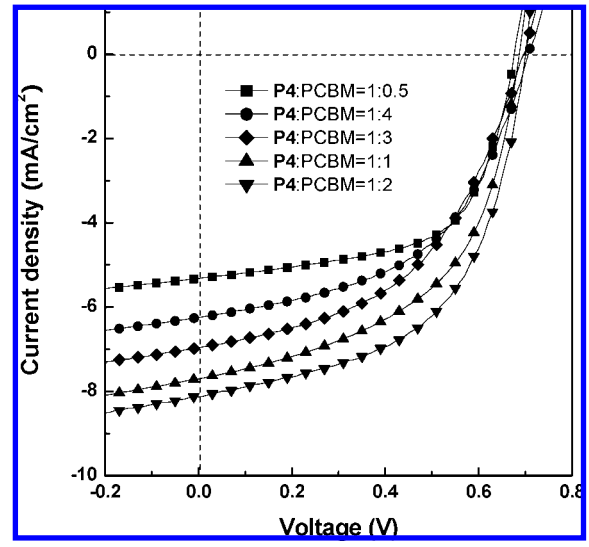

Figure 6. $I-V$ curves of PSC devices containing an active layer of **P4**:PCBM (w/w) with different weight ratios under simulated AM 1.5 solar irradiation.

Table 5. Photovoltaic Parameters[a] for Bulk-Heterojunction PSC Devices Containing Different Weight Ratios of Blended Copolymer P4:PCBM

weight ratios of blended **P4**:PCBM	V_{oc} (V)	I_{sc} (mA/cm^2)	FF (%)	PCE (%)
1:0.5	0.675	5.32	61.0	2.19
1:1	0.683	7.70	53.0	2.79
1:2	0.700	8.00	53.7	3.04
1:3	0.700	6.96	48.3	2.35
1:4	0.705	6.25	51.0	2.25

[a] PSC devices with the configuration of ITO/PEDOT:PSS/Polymer:PCBM/Ca/Al were measured under AM 1.5 irradiation, 100 mW/cm^2.

Conclusions

Using the concept of incorporating electron-withdrawing groups in the donor−acceptor conjugated copolymers, we have successfully synthesized six cyclopentadithiophene-bithiazole-based copolymers (**P1**−**P6**) employing oligo(bithiazole), bithiazole−oligo(thiophene), and diarylene−cyanovinylene−bithiazole groups by palladium(0)-catalyzed Stille coupling reactions. The band gaps and HOMO/LUMO levels of these resulting copolymers can be finely tuned as demonstrated in the exploration of optical absorption and electrochemical properties. In powder X-ray diffraction (XRD) measurements, these copolymers exhibited obvious diffraction features indicating highly ordered $\pi-\pi$ stacking in the solid state. These copolymers also showed excellent charge-transporting properties with hole mobilities of (3.3−5.6) × 10^{-4} cm^2 V^{-1} s^{-1} and good processabilities for PSC applications. A preliminary PSC device based on the blended copolymer **P4**:PCBM = 1:2 (w/w) had the maximum power conversion efficiency (PCE) value up to

3.04%, which gave the best photovoltaic performance with the values of $I_{sc} = 8.00$ mA/cm^2, FF = 53.7%, and $V_{oc} = 0.70$ V as well as a peak EQE value of 60% under simulated AM1.5 solar illumination. These copolymers demonstrate a novel family of conjugated copolymers along the path toward achieving low cost PSC applications. Currently, deeper investigation for better photovoltaic properties is underway to further optimize the PSC performance.

Acknowledgment. We are grateful to the National Center for High-performance Computing for computer time and facilities. The powder XRD measurements are supported by beamline BL17A (charged by Dr. Jey-Jau Lee) of the National Synchrotron Radiation Research Center (NSRRC), in Taiwan. The financial supports of this project provided by the National Science Council of Taiwan (ROC) through NSC 96-2113-M-009-015, National Chiao Tung University through 97W807, Energy and Environmental Laboratories (charged by Dr. Chang-Chung Yang) in Industrial Technology Research Institute (ITRI), and Chung-Shan Institute of Science and Technology (in Taiwan) are acknowledged.

Supporting Information Available: Text giving synthetic procedures and characterization for compounds **2**−**6**, **8**−**10**, and **13**−**14** and experimental details for XRD characterization and figures showing photoluminescence spectra of copolymers **P1**−**P6** and schematic representation of proposed layered and packing models of copolymers **P1**−**P6**. This material is available free of charge via the Internet at http://pubs.acs.org.

References and Notes

(1) Yu, G.; Gao, J.; Hummelen, J. C.; Wudl, F.; Heeger, A. J. *Science* **1995**, *270*, 1789–1791.

(2) Thompson, B. C.; Fréchet, J. M. J. *Angew Chem., Int. Ed.* **2008**, *47*, 58–77. (b) Kietzke, T.; Shin, R. Y. C.; Egbe, D. A. M.; Chen, Z.-K.; Sellinger, A *Macromolecules* **2007**, *40*, 4424–4428. (c) Uhrich, C.; Schueppel, R.; Petrich, A.; Pfeiffer, M.; Leo, K.; Brier, E.; Kilickiran, P.; Baeuerle, P. *Adv. Funct. Mater.* **2007**, *17*, 2991–2999. (d) McNeill, C. R.; Abrusci, A.; Zaumseil, J.; Wilson, R.; McKiernan, M. J.; Burroughes, J. H.; Halls, J. J. M. *Appl. Phys. Lett.* **2007**, *90*, 193506–3.

(3) Bouclé, J.; Ravirajanac, P.; Nelson, J. *J. Mater. Chem.* **2007**, *17*, 3141–3153. (b) Beek, W. J. E.; Wienk, M. M.; Janssen, R. A. J *Adv. Funct. Mater.* **2006**, *16*, 1112–1116. (c) Moet, D. J. D.; Koster, L. J. A.; de Boer, B.; Blom, P. W. M. *Chem. Mater.* **2007**, *19*, 5856–5861. (d) Beek, W. J. E.; Wienk, M. M.; Janssen, R. A. J. *Adv. Mater.* **2004**, *16*, 1009–1013.

(4) (a) Li, G.; Shrotriya, V.; Huang, J.; Yao, Y.; Moriarty, T.; Emery, K.; Yang, Y. *Nat. Mater.* **2005**, *4*, 864–868. (b) Koppe, M.; Scharber, M.; Brabec, C.; Duffy, W.; Heeney, M.; McCulloch, I. *Adv. Funct. Mater.* **2007**, *17*, 1371–1376. (c) Ma, W.; Yang, C.; Gong, X.; Lee, K.; Heeger, A. J. *Adv. Funct. Mater.* **2005**, *15*, 1617–1622.

(5) (a) Hou, J. H.; Tan, Z.; Yan, Y.; He, Y.; Yang, C.; Li, Y. *J. Am. Chem. Soc.* **2006**, *128*, 4911–4916. (b) Chang, Y. T.; Hsu, S. L.; Chen, G. Y.; Su, M. H.; Singh, T. A.; Diau, E. W. G.; Wei, K. H. *Adv. Funct. Mater.* **2008**, *18*, 1–10. (c) Demadrille, R.; Delbosc, N.; Kervella, Y.; Firon, M.; Bettignies, R. D.; Billon, M.; Rannou, P; Pron, A. *J. Mater. Chem.* **2007**, *17*, 4661–4669. (d) Qin, Y.; Kim, J. Y.; Frisbie, C. D.; Hillmyer, M. A. *Macromolecules* **2008**, *41*, 5563–570.

(6) (a) Hou, J. H.; Park, M.-H.; Zhang, S.; Yao, Y.; Chen, L.-M.; Li, J.-H.; Yang, Y. *Macromolecules* **2008**, *41*, 6012–6018. (b) Chan, S. H.; Chen, C. P.; Chao, T. C.; Ting, C.; Lin, C. S.; Ko, B. T. *Macromolecules* **2008**, *41*, 5519–5526. (c) Zhan, X.; Tan, Z.; Domercq, B.; An, Z.; Zhang, X.; Barlow, S.; Li, Y.; Zhu, D.; Kippelen, B.; Marder, S. R. *J. Am. Chem. Soc.* **2007**, *129*, 7246–7247. (d) Liu, C. L.; Tsai, J. H. ; Lee, W. Y.; Chen, W. C.; Jenekhe, S. A. *Macromolecules* **2008**, *41*, 6952–6959.

(7) Coppo, P.; Turner, M. L. *J. Mater. Chem.* **2005**, *15*, 1123–1133.

(8) (a) Kraak, A.; Wieserma, A. K.; Jordens, P.; Wynberg, H. *Tetrahedron* **1968**, *24*, 3381–3398. (b) Berlin, A.; Brenna, E.; Pagani, G. A.; Sannicolo, F. *Synth. Met.* **1992**, *51*, 287–297. (c) Cunningham, D. D.; Gaa, A.; Pham, C. V.; Lewis, E. T.; Burkhardt, A.; Davidson, L. L.; Kansah, A. N.; Ataman, O. Y.; Zimmer, H.; Mark, H. B *J. Electrochem. Soc.* **1988**, *135*, 2750.

(9) (a) Zotti, G.; Schiavon, G. *Macromolecules* **1994**, *27*, 1938–1942. (b) Asawapirom, U.; Scherf, U. *Macromol. Rapid Commun.* **2001**, *22*, 746–749. (c) Coppo, P.; Cupertino, D. C.; Yeates, S. G.; Turner, M. L. *Macromolecules* **2003**, *36*, 2705–2711. (d) Cremer, L. D.; Vandeleene, S.; Maesen, M.; Verbiest, T.; Koeckelberghs, G. *Macromolecules* **2008**, *41*, 591–598.

(10) (a) Zhang, M.; Tsao, H. N.; Pisula, W.; Yang, C.; Mishra, A. K.; Müllen, K. *J. Am. Chem. Soc.* **2007**, *129*, 3472–3473. (b) Mü1hlbacher, D.; Scharber, M.; Morana, M.; Zhu, Z.; Waller, D.; Gaudiana, R.; Brabec, C. *Adv. Mater.* **2006**, *18*, 2884–2889.

(11) (a) Lee, J. K.; Ma, W. L.; Brabec, C. J.; Yuen, J.; Moon, J. S.; Kim, J. Y.; Lee, K.; Bazan, G. C.; Heeger, A. J. *J. Am. Chem. Soc.* **2008**, *130*, 3619–3623. (b) Peet, J.; Kim, J. Y.; Coates, N. E.; Ma, W. L.; Moses, D.; Heeger, A. J.; Bazan, G. C. *Nat. Mater.* **2007**, *6*, 497–500. (c) Zhu, Z.; Waller, D.; Gaudiana, R.; Morana, M.; Mü1hlbacher, D.; Scharber, M.; Brabec, C. *Macromolecules* **2007**, *40*, 1981–1986. (d) Mouleì, A. J.; Tsami, A.; Bünnagel, T. W.; Forster, M.; Kronenberg, N. M.; Scharber, M.; Koppe, M.; Morana, M.; Brabec, C. J.; Meerholz, K.; Scherf, U. *Chem. Mater.* **2008**, *20*, 4045–4050. (e) Xiao, S.; Zhou, H.; You, W. *Macromolecules* **2008**, *41*, 5688–5696.

(12) (a) Osaka, I.; Sauvé, G.; Zhang, R.; Kowalewski, T.; McCullough, R. D. *Adv. Mater.* **2007**, *19*, 4160–4165. (b) Naraso Wudl, F. *Macromolecules* **2008**, *41*, 3169–3174. (c) Cao, J.; Kampf, J. W.; Curtis, M. D. *Chem. Mater.* **2003**, *15*, 404–411. (d) Yamamoto, T.; Arai, M.; Kokubo, H.; Sasaki, S. *Macromolecules* **2003**, *36*, 7986–7993. (e) Politis, J. K.; Curtis, M. D.; Gonzalez, L.; Martin, D. C.; He, Y.; Kanicki, J. *Chem. Mater.* **1998**, *10*, 1713–1719. (f) Mamada, M.; Nishida, J.; Kumaki, D.; Tokito, S. *Chem. Mater.* **2007**, *19*, 5404–5409.

(13) (a) Yasuda, T.; Sakai, Y.; Aramaki, S.; Yamamoto, T. *Chem. Mater.* **2005**, *17*, 6060–6068. (b) Yamamoto, T.; Suganuma, H.; Maruyama, T.; Inoue, T.; Muramatsu, Y.; Arai, M.; Komarudin, D.; Ooba, N.; Tomaru, S.; Sasaki, S.; Kubota, K. *Chem. Mater.* **1997**, *9*, 1217–1225. (c) Yamamoto, T.; Otsuka, S.; Namekawa, K.; Fukumoto, H.; Yamaguchi, I.; Fukuda, T.; Asakawa, N.; Yamanobe, T.; Shiono, T.; Cai, Z. *Polymer* **2006**, *47*, 6038–6041.

(14) (a) Lee, J.; Jung, B. J.; Lee, S. K.; Lee, J. I.; Cho, H. J.; Shim, H. K. *J. Polym. Sci., Part A: Polym. Chem.* **2005**, *43*, 1845–1857. (b) Wong, W. Y.; Wang, X. Z.; He, Z.; Chan, K. K.; Djurii, A. B.; Cheung, K. Y.; Yip, C. T.; Ng, A. M. C.; Xi, Y. Y.; Mak, C. S. K.; Chan, W. K. *J. Am. Chem. Soc.* **2007**, *129*, 14372–14380.

(15) (a) Roncali, J. *Macromol. Rapid Commun.* **2007**, *28*, 1761–1775. (b) van Mullekom, H. A. M.; Vekemans, J. A. J. M.; Havinga, E. E.; Meijer, E. W. *Mater. Sci. Eng.* **2001**, *32*, 1–40.

(16) (a) Brabec, C. J.; Sariciftci, N. S.; Hummelen, J. C. *Adv. Funct. Mater.* **2001**, *11*, 15–26. (b) Chen, C. P.; Chan, S. H.; Chao, T. C.; Ting, C.; Ko, B. T. *J. Am. Chem. Soc.* **2008**, *130*, 12828–12833.

(17) (a) Shrotriya, V.; Li, G.; Yao, Y.; Chu, C. W.; Yang, Y. *Appl. Phys. Lett.* **2006**, *88*, 073508. (b) Malliaras, G. G.; Salem, J. R.; Brock, P. J.; Scott, C. *Phys. Rev. B* **1998**, *58*, 13411. (c) Chirvase, D.; Chiguvare, Z.; Knipper, M.; Parisi, J.; Dyakonov, V.; Hummelen, J. C. *Phys. Rev. B* **2004**, *70*, 235207.

(18) Lin, H. C.; Lee, K. W.; Tsai, C. M.; Wei, K. H. *Macromolecules* **2006**, *39*, 3808–3816.

(19) (a) Lucas, P.; El Mehdi, N.; Anh Ho, H.; Belanger, D.; Breau, L. *Synthesis* **2000**, *9*, 1253–1258. (b) Brzezinski, J. Z.; Reynolds, J. R. *Synthesis* **2002**, *8*, 1053–1056. (c) Coppo, P.; Cupertino, D. C.; Yeates, S. G.; Turner, M. L. *Macromolecules* **2003**, *36*, 2705–2711.

(20) (a) Cremer, L. D.; Vandeleene, S.; Maesen, M.; Verbiest, T.; Koeckelberghs, G. *Macromolecules* **2008**, *41*, 591–598. (b) Liao, L.; Dai, L.; Smith, A.; Durstock, M.; Lu, J.; Ding, J.; Tao, Y. *Macromolecules* **2007**, *40*, 9406–9412.

(21) (a) McCulloch, I.; Heeney, M.; Bailey, C.; Genevicius, K.; MacDonald, I.; Shkunov, M.; Sparrowe, D.; Tierney, S.; Wagner, R.; Zhang, W.; Chabinyc, M. L.; Kline, R. J.; McGehee, M. D.; Toney, M. F. *Nat. Mater.* **2006**, *5*, 328–333. (b) Ong, B. S.; Wu, Y.; Liu, S.; Gardner, S. *J. Am. Chem. Soc.* **2004**, *126*, 3378–3379. (c) Zhao, N.; Botton, G. A.; Zhu, S.; Duft, A.; Ong, B. S.; Wu, Y.; Liu, P. *Macromolecules* **2004**, *37*, 8307–8312.

(22) (a) Lu, J.; Xia, P. F.; Lo, P. K.; Tao, Y.; Wong, M. S. *Chem. Mater.* **2006**, *18*, 6194–6203. (b) Ma, W.; Yang, C.; Gong, X.; Lee, K.; Heeger, A. J. *Adv. Funct. Mater.* **2005**, *15*, 1617–1622.

(23) (a) Liao, L.; Dai, L.; Smith, A.; Durstock, M.; Lu, J.; Ding, J.; Tao, Y. *Macromolecules* **2007**, *40*, 9406–9412. (b) Zhu, Y.; Champion, R. D.; Jenekhe, S. A. *Macromolecules* **2006**, *39*, 8712–8719.

(24) (a) Colladet, K.; Fourier, S.; Cleij, T. J.; Lutsen, L.; Gelan, J.; Vanderzande, D.; Huong Nguyen, L.; Neugebauer, H.; Sariciftci, S.; Aguirre, A.; Janssen, G.; Goovaerts, E. *Macromolecules* **2007**, *40*, 65–72. (b) Roncali, J. *Macromol. Rapid Commun.* **2007**, *28*, 1761–1775. (c) Galand, E. M.; Kim, Y.-G.; Mwaura, J. K.; Jones, A. G.; McCarley, T. D.; Shrotriya, V.; Yang, Y.; Reynolds, J. R. *Macromolecules* **2006**, *39*, 9132–9142.

(25) Shahid, M.; Ashraf, R. S.; Klemm, E.; Sensfuss, S. *Macromolecules* **2006**, *39*, 7844–7853.

(26) (a) Chang, Y. T.; Hsu, S. L.; Su, M. H.; Wei, K. H. *Adv. Funct. Mater.* **2007**, *17*, 3326–3331. (b) Giacalone, F.; Segura, J. L.; Martín, N.; Catellani, M.; Luzzati, S.; Lupsac, N. *Org. Lett.* **2003**, *5*, 1669–1672.
(27) Mihailetchi, V. D.; Duren, J. K. J. v.; Blom, P. W. M.; Hummelen, J. C.; Janssen, R. A. J.; Kroon, J. M.; Rispens, M. T.; Verhees, W. J. H.; Wienk, M. M. *Adv. Funct. Mater.* **2003**, *13*, 43–46.
(28) (a) Letizia, J. A.; Salata, M. R.; Tribout, C. M.; Facchetti, A.; Ratner, M. A.; Marks, T. J. *J. Am. Chem. Soc.* **2008**, *130*, 9679–9694. (b) Lu, G.; Usta, H.; Risko, C.; Wang, L.; Facchetti, A.; Ratner, M. A.; Marks, T. J. *J. Am. Chem. Soc.* **2008**, *130*, 7670–7685.
(29) (a) Street, R. A. *Nat. Mater.* **2006**, *5*, 171–172. (b) Kokubo, H.; Sato, T.; Yamamoto, T. *Macromolecules* **2006**, *39*, 3959–3963. (c) Yamamoto, T.; Komarudin, D.; Arai, M.; Lee, B. L.; Suganuma, H.; Asakawa, N.; Inoue, Y.; Kubota, K.; Sasaki, S.; Fukuda, T.; Matsuda, H. *J. Am. Chem. Soc.* **1998**, *120*, 2047–2058. (d) Chen, T. A.; Wu, X.; Rieke, R. D. *J. Am. Chem. Soc.* **1995**, *117*, 233–244.
(30) (a) Savenije, T. J.; Kroeze, J. E.; Yang, X. N.; Loos, J. *Adv. Funct. Mater.* **2005**, *15*, 1260–1266. (b) Baek, N. S.; Hau, S. K.; Yip, H. L.; Acton, O.; Chen, K. S.; Jen, A. K. Y. *Chem. Mater.* **2008**, *20*, 5734–5736.
(31) (a) Günes, S.; Neugebauer, H.; Sariciftci, N. S. *Chem. Rev.* **2007**, *107*, 1324–1338. (b) Scharber, M. C.; Mühlbacher, D.; Koppe, M.; Denk, P.; Waldauf, C.; Heeger, A. J.; Brabec, C. J. *Adv. Mater.* **2006**, *18*, 789–794. (c) Brabec, C. J.; Cravino, A.; Meissner, D.; Sariciftci, N. S.; Fromherz, T.; Rispens, M. T.; Sanchez, L.; Hummelen, J. C. *Adv. Funct. Mater.* **2001**, *11*, 374–380.
(32) (a) Huang, J. H.; Ho, Z. Y.; Kekuda, D.; Chang, Y.; Chu, C. W.; Ho, K. C. *Nanotechnology* **2009**, *20*, 025202.
(33) (a) Li, G.; Shrotriy, V.; Yao, Y.; Huang, J.; Yang, Y. *J. Mater. Chem.* **2007**, *17*, 3126–3140.

MA900416D